Published in final edited form as:

Nanomedicine. 2016 April ; 12(3): 677–687. doi:10.1016/j.nano.2015.11.002.

Nanoparticle Surface Charge Impacts Distribution, Uptake and Lymph Node Trafficking by Pulmonary Antigen-Presenting Cells

Catherine A. Fromen[1], **Tojan B. Rahhal**[2], **Gregory R. Robbins**[3,4], **Marc P. Kai**[1], **Tammy W. Shen**[2], **J. Christopher Luft**[2,4], and **Joseph M. DeSimone**[1,2,4,5]

[1] Department of Chemical and Biomolecular Engineering, North Carolina State University, Raleigh, NC 27695.

[2] Eshelman School of Pharmacy, University of North Carolina at Chapel Hill, Chapel Hill, NC 27599.

[3] Department of Microbiology-Immunology, University of North Carolina at Chapel Hill, Chapel Hill, NC 27599.

[4] Lineberger Comprehensive Cancer Center, University of North Carolina at Chapel Hill, Chapel Hill, NC 27599.

[5] Department of Chemistry, University of North Carolina at Chapel Hill, Chapel Hill, NC 27599.

Abstract

Engineered nanoparticles have the potential to expand the breadth of pulmonary therapeutics, especially as respiratory vaccines. Notably, cationic nanoparticles have been demonstrated to produce superior local immune responses following pulmonary delivery; however, the cellular mechanisms of this increased response remains unknown. To this end, we systematically investigated the cellular response of lung APCS following pulmonary instillation of anionic and cationic charged nanoparticles. While nanoparticles of both surface charges were capable of trafficking to the draining lymph node and were readily internalized by alveolar macrophages, both CD11b and CD103 lung dendritic cell (DC) subtypes preferentially associated with cationic nanoparticles. Instillation of cationic nanoparticles resulted in the upregulation of *Ccl2* and *Cxc10*, which likely contributes to the recruitment of CD11b DCs to the lung. In total, these cellular mechanisms explain the increased efficacy of cationic formulations as a pulmonary vaccine carrier and provide critical benchmarks in the design of pulmonary vaccine nanoparticles.

Graphical Abstract

Nanoparticle surface charge is a key parameter in the recruitment and association of pulmonary antigen presenting cells following respiratory administration, resulting in increased cytokine and

Joseph M. DeSimone Department of Chemistry, The University of North Carolina at Chapel Hill, CB# 3290, 257 Caudill Labs, Chapel Hill, NC 27599-3290, DeSimone@unc.edu, Tel: (919) 962-2166, Fax: (919) 962-5467.

Conflict of Interest: J.M.D. is a founder and maintains a financial interest in Liquidia Technologies.

chemokine production necessary for an effective lung vaccine. Pulmonary delivery of PRINT® cationic nanoparticles resulted in an increased local immune response and preferential association with dendritic cells compared to PRINT® anionic nanoparticle administration.

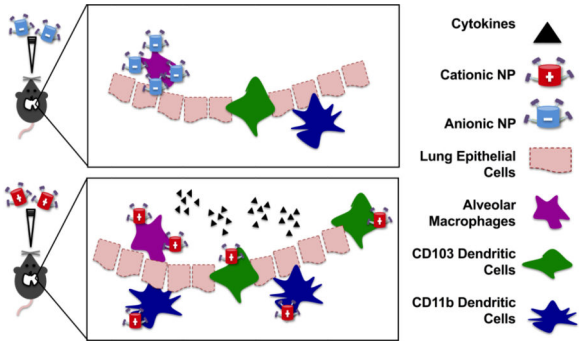

Keywords

nanoparticle; lung; dendritic cell; pulmonary drug delivery; vaccine

INTRODUCTION

The next generation of vaccines can be achieved by pulmonary delivery of precision-engineered particles (1-8). Engineered micro- and nanoparticles (NP) offer elegant solutions for pathogen mimicry, while providing increased safety and efficacy over current vaccine strategies (2, 3, 6). Additionally, engineered particles can be designed such that aerosol properties, lung deposition, and cellular interactions are independently taken into consideration (1, 2, 8, 9). While there is extensive literature describing how physical particle properties can influence aerodynamic diameter and thus pulmonary deposition, there is minimal understanding of how these same particle properties influence interactions with lung cells and their subsequent immune responses (1, 9).

Amongst the numerous cell types present in the lung, of particular interest to vaccine design are antigen presenting cells (APCs), which comprise B cells, dendritic cells (DCs) and macrophages (3, 10-15). Alveolar macrophages (AM), the main phagocytic cell in the lung, roam the airway epithelium, where they are responsible for internalizing, sequestering, and digesting any foreign material (12, 16-18). While they are generally considered APCs, their main function in the lung is more maintenance and clearance, rather than initiating adaptive responses (12, 17, 18). In contrast, lung DCs are considered “professional” APCs and act as a sentinel in the lung, monitoring and sampling foreign material to mount adaptive immune responses (3, 14, 15). Lung DCs are responsible for internalizing foreign particulates, digesting and presenting antigen by major histocompatibility complex (MHC) II, migrating to lymph nodes (LNs), and educating T cells (11-15, 19-21). In the lung, there are two conventional myeloid-derived DC subsets, CD11b and CD103 DCs, which have distinct functions (12, 14, 22). CD103 DCs protrude through the lung epithelium, are considered the main migratory population, and have been implicated in skewing the lung towards Th1, Th2 and Th17 responses given different stimuli (12, 14, 16, 20-24). While CD11b DCs can also

migrate to the LNs, they have been shown to prime IgA production in the lung and are the major producers of soluble protein mediators, chemokines, and cytokines (11, 14, 16, 19, 23, 24). These cells are found predominately under the basement membrane in the conducting airways (12). NP vaccination strategies capable of preferentially targeting these DCs subtypes, while avoiding inevitable AM uptake, are expected to result in superior responses.

Nanoparticles have been explored as pulmonary vaccine carriers, due to their potential to diffuse through mucosa, their avoidance of AMs, and their ability to co-deliver both adjuvants and antigens (3, 5-7, 10, 16, 25). To date, the role of NP charge on lung APC association remains poorly understood, as the majority of vaccination studies have focused on anionic NP carriers (4, 5). These formulations follow design principles of pathogen mimicry, as the majority of both bacteria and viruses have surfaces with acidic isoelectric points (26, 27). However, recent work from our group has demonstrated that pulmonary vaccination with cationic NPs can enhance local and systemic antibody production to a model antigen, as compared to otherwise equivalent anionic NPs (8). While these results indicate that nanoparticle charge is a key variable to immune responses in the lung, the underlying cellular mechanisms responsible for this deviation in immune response remain unclear. Understanding these lung processes is critical in the ultimate identification of NP design features capable of producing an optimized, controlled immune response.

As such, the goal of this work is to understand the cellular lung mechanisms involved in the processing of cationic and anionic NPs. We hypothesized that increased antibody production was the result of increased association of cationic NPs with lung DC subtypes, as well as a slight adjuvant effect of the charge associated with the NP itself. To further elucidate the role of nanoparticle surface charge on increased immune activity in the lung, we utilized the Particle Replication In Non-wetting Templates (PRINT) technique to fabricate hydrogel-based NPs that varied only in surface charge and otherwise had identical size, shape and antigen loading. We investigate the role of NP charge on uptake by APCs, cytokine and chemokine recruitment, and subsequent trafficking of NPs to the mediastinal LNs in order to identify key cellular mechanisms involved in lung NP immune responses.

METHODS

Animals

All studies were conducted in accordance with National Institutes of Health guidelines for the care and use of laboratory animals and approved by the Institutional Animal Care and Use Committee (IACUC) at UNC. C57BL/6 (Jackson Laboratories) were maintained in pathogen-free facilities at UNC and used between 8-15 wks.

Nanoparticle Fabrication

Amine-containing 80 nm × 320 nm hydrogel rod-shaped (ζ+)NP were fabricated on a continuous roll-to-roll PRINT method as described previously (28) and in detail in Supplemental Methods. (ζ+)NPs in DMF were incubated with 100 M excess succinic anhydride for 30 minutes, washed first with borate buffer pH 9.5 and then three additional washes in water to achieve (ζ-)NP. Ovalbumin (OVA) functionalization was achieved using

water-soluble carboiimide chemistry, described previously (8) and in Supplemental Methods. NP characterization is described in Supplemental Methods.

Pulmonary Administration

NP and control formulations were delivered to the lungs of anesthetized mice through an orotracheal instillation in a 50 μL volume in PBS (8, 29). NP doses were 100 μg NP/mouse, corresponding to 10 μg OVA/mouse which was used as the control soluble OVA dose. In studies with adjuvant, 2.5 μg CpG/mouse or 20 μg LPS/mouse was delivered.

Biodistribution Study

Female, C57BL/6 mice (n=4) were dosed 88 μg of the respective nanoparticle (positive or negative 80 nm × 320 nm Dylight 650 hydrogels) orotracheally, as described above. As described detail within Supplemental Methods, blood and bronchoalveolar lavage fluid (BALF) were collected at 24 and 72 hrs with a single 1 mL PBS flush. Organs were then harvested for IVIS® Lumina optical imaging (Caliper Life Sciences, emission filter Cy5.5 and excitation filter 640 nm) and radiant efficiency per gram was determined. Following harvest, lungs were dissociated into a single cell suspension, placed in TRIzol® (Invitrogen) and stored before extracting RNA for RT-qPCR.

Quantitative Real-Time PCR (qRT-PRC)

Mouse lungs from biodistribution study were used for qRT-PCR analysis. RNA isolation was performed from single cell suspensions of whole lung cells using TRIzol® (Invitrogen) followed by reverse transcription per standard protocol (30) and described in Supplemental Methods.

Antibodies: Flow Cytometry, ELISAs, and Histology

Single cell suspensions from tissues (see Supplemental Methods) were kept on ice and blocked with anti-CD16/32 (Fc block, eBioscience) and stained with the following antibodies to mouse cell surface molecules; I-A/I-E-PE-Cy7, CD11b-APC-Cy7, CD11c-PB, F4/80-PE-Cy5, CD45-BV510, CD103-PE, CD3-BV510, CD19-PE-Cy7, were from BioLegend. Cells were fixed using 2% PFA in PBS. All data were collected using LSRII (BD Biosciences) flow cytometer and analyzed using FlowJo software (Tree Star). Briefly, in the lung, macrophages and DCs were identified as $CD45^{+}CD11c^{+}$ populations and were separated by MHC II expression. MHC II^{lo} macrophages were confirmed to be $F4/80^{+}$ and $CD11b^{-}$. MHC II^{hi} DCs were further separated into a $CD103^{+}$, $CD11b^{-}$ population, identifying the CD103 DCs, and a $CD103^{-}CD11b^{+}$ population of CD11b DCs. In the LN, T and B cells were identified as $CD3^{+}$ and $CD19^{+}$, while DCs were identified as $CD3^{-}CD19^{-}CD11c^{+}$. The two DC subtypes were separated by CD103 and CB11b, as before. Representative gating for the lung and LN is shown in Supplemental Figures 1 and 5, respectively. Following population identification, each cell population was analyzed for NP fluorescence, gated by the PBS-treated, NP fluorescence-minus one (FMO) control (31). NP association was quantified as the percentage of each cell type which had a detectable signal in the NP channel. From the NP positive gate, the median fluorescence intensity (MFI) per cell was also determined.

Enzyme-linked immunosorbent assay (ELISA) kits for IL-6, TNF-α, and IL-1β were purchased from BD Biosciences and used following manufacturer's suggestions on BALF and Serum samples. Preparation of lung histology is described in Supplemental Methods.

Statistical Analysis

Statistical analyses were performed with GraphPad Prism version 6. Analysis of groups was performed as indicated in figures, where asterisks indicating p values of *≤0.05, **≤0.01, ***≤0.001 and n.s indicating not significant. NP batches, cell assays, and immunization studies were repeated in at least two independent experiments, with the number of replicates (NPs, cells, mice) indicated in figures.

RESULTS

Distribution of Cationic and Anionic Formulations in the Lung Following Pulmonary Instillation

In order to compare anionic and cationic NPs, we first quantified bulk organ distribution following pulmonary instillation in mice. Nanoparticles of (ζ+)NP and (ζ-)NP were fabricated as described previously (8) with the addition of a fluorescent dye to enable visualization throughout the organ tissue using an IVIS imaging system. Examples of lung fluorescence images are shown in Figure 1A. Organs were resected at 24 and 72 hrs to determine NP localization within this timeframe (Figure 1B). At both time points, NP fluorescence was detected above baseline in the lung and mediastinal lymph nodes, with no statistical difference between these groups. This indicated that NPs were mainly retained in the lung, with a detectable amount trafficking to the draining lymph node, even within 24 hrs.

Lung pathology on mice receiving either (ζ+)NP or (ζ-)NP administration was performed to observe the localization of fluorescent NPs in the airways at 72 hrs (Figure 2). Both NP types were observed throughout the entire lung and most often appear as punctate fluorescent regions, presumably internalized into phagocytic cells. These sections were stained for $CD11c^+$, finding that the majority of the punctate fluorescence corresponded with this surface marker.

To further differentiate the $CD11c^+$ cells visually associated with NPs, we utilized flow cytometry to quantify NP uptake in three critical APC lung populations: AM, CD11b DCs and CD103 DCs. We sought to explore differences in cell associations of NP and NP-OVA formulations of both charges in isolated whole lung cells at 72 hrs following instillation of fluorescently-labeled NPs. Ovalbumin (OVA) was used as a model antigen to observe if this enhanced uptake. The percentage of NP^+ cells indicates how likely a given cell type is to associate with any amount of NPs, while the MFI lends insight to how many NPs each individual cell internalizes. The total fluorescence was calculated by multiplying the number of positive NP cells by the MFI in order to give an overall view of the total volume (related to mass) of NPs internalized; the magnitude of this value allows for comparison between NP doses and cell types to quantify cellular distribution (Figure 3). Representative gating used to analyze these populations is shown in Supplemental Figure 1.

Alveolar macrophages readily internalized both anionic and cationic NPs (Figure 3A left). At the NP dose given, between 60-100% of AMs were NP^+. This corresponds well with the known function of AM as the primary phagocytic cell in the lung. Interestingly, a greater percentage of AM internalized (ζ-)NPs. This is further evident in the MFI and total fluorescence intensity (FI) of these cells, as (ζ-)NP-OVA and (ζ-)NP were a factor of 10 higher than the corresponding (ζ+)NPs (Figure 3A middle, right). This indicates that a single AM internalized a significantly greater number of anionic NPs, suggesting that either AM have a preference towards internalization of anionic NPs, or the total availability of dosed NPs was greater than (ζ+)NPs, presumably due to other clearance methods or non-specific binding.

While the AMs showed preference to anionic NPs, both DC subtypes show increased association with cationic NPs. Slight increases in NP^+ populations were observed following (ζ+)NP-OVA and (ζ+)NP administration for CD103 and CD11b DCs (Figure 3B and 3C respectively). A greater percentage of CD11b DCs were found to associate with (ζ+)NPs. Overall, a greater percentage of CD11b DCs were NP^+ as compared to CD103 DCs, indicating CD11b DCs found in the lung are more likely to associate with NPs at this time point. Interestingly, greater association was observed for non-functionalized NPs, as both CD103 and CD11b DCs showed a decrease in (ζ+)NP-OVA association when compared to (ζ+)NP. However, both of these groups were higher than anionic formulations. Unlike the AM, the MFI of both NP^+ CD103 or CD11b DCs were not statistically different across the treatment groups, indicating an equivalent amount of NP internalization per cell (Figure 3B and C, middle). Compared to AM, the MFI intensity in both DC subtypes was considerably lower as well, indicating that DCs in general associated with fewer numbers of NPs. Total fluorescence intensity between DC subtypes collected in the lung (Figure 3B and C, right) indicates that CD11b DCs in general associate with a greater amount of NPs than CD103 DCs, with (ζ+)NPs, and (ζ+)NP-OVA to a lesser extent, showing the greatest association.

Effects of Nanoparticle Treatment on Cellular Responses in the Lung

Differences between NP associations with different lung APCs were observed with flow cytometry, which can, in part, explain differences previously observed following vaccination with these two formulations (8). We further hypothesized that the (ζ+)NP may have an adjuvant-like effect in the lung upon administration, which would contribute to production of local antibody responses upon vaccination.

To test this, mouse lungs were treated with both NP types and tested for cytokine production in the BALF, with PBS and CpG (a toll-like receptor, TLR, 9 agonist) as negative and positive controls. The CpG dose delivered was equivalent to previous co-delivery NP-adjuvant vaccination strategies and served as a qualitative control of known adjuvant activity (5, 8). No significant increase in IL-6 (Figure 4A), TNF-α, or IL-1β (not shown) levels in the BALF over saline treatment were found at 24 and 72 hrs. This was in stark contrast to the effect of CpG administration to the lung, which resulted in ~1000 fold increase in inflammatory cytokine production at both time points. Minimal increase, if any, in systemic production of these same inflammatory markers was observed for all treatment types (Figure 4B). This indicates that both formulations of NPs have no increase in local or systemic

inflammation over three days, a time point anticipated to be sufficient in capturing the onset of acute inflammation. The lack of acute inflammatory responses was corroborated by immunohistochemistry staining of NP-treated lungs. H&E staining of representative lung histology at 24 hrs (shown in Figure 4C and D) and 72 hrs (not shown), shows no evidence of leukocyte recruitment to the lung vasculature. Finally, we tested if (ζ+)NP administration would be detrimental to lung function, as previous studies have already shown that (ζ-)NPs are well tolerated (32). As shown in Supplemental Figure 2, lungs pretreated with (ζ+)NPs maintained the ability to mount an appropriate inflammatory response upon LPS stimulation.

While no significant differences in cytokine levels secreted in the BALF were detected, we hypothesized that administration of either (ζ+)NP or (ζ-)NP may result in subtle changes in cytokine and chemokine production within the lung. At 24 and 72 hrs following instillation, whole lungs were homogenized into a single cell suspension to perform qRT-PCR and to observe relevant cytokines and chemokines at the mRNA level, normalized to *Gapdh* (see Supplemental Figure 3 for quantified expression). Mice treated with LPS at 24 hrs were included as a reference of a known soluble mediator of inflammation; this group was excluded from our statistical analysis as it is a qualitative, and not quantitative control, and LPS inflammatory responses at the mRNA level are known to have resolved in C57BL/6 mice within 24 hrs (33). As shown in Figure 5, lungs treated with (ζ+)NPs were found to result in significant increased expression over untreated (UT) controls for *Ccl2* and *Cxcl10* at both 24 and 72 hrs, as well as increased expression at 24 hrs for *Il-10*, *Il-4*, *Il-6*, *Ifn-γ*, and *Il-12β.* In these cytokines, mRNA expression had returned to basal expression by 72 hrs, indicating an acute and not sustained response to (ζ+)NPs. In contrast, lungs treated with (ζ-)NPs showed no increased expression of any of these markers when compared to UT controls. No increase in expression was observed from either NP type for *Tnf-α* (Figure 5), *Tgfβ-1,* or *Il-12α* (Supplemental Figure 4).

Both *Ccl2* and *Cxcl10* are important chemo-attractants involved in DC recruitment to the lungs (34-36). As these were upregulated in lungs treated with (ζ+)NPs at both 24 and 72 hrs, we sought to identify changes in lung populations following NP administration after 72 hrs, allowing for a maximal effect to be detected. Using flow cytometry to differentiate AM and DC subtypes as before, we observed relative differences in the total percentage of $CD45^+$ leukocytes (Figure 6A), as well as the proportion of DCs between CD11b and CD103 subtypes (Figure 6B). Interestingly, there are no statistical differences in the relative percentage of AM of total $CD45^+$ cells, but the relative percentage of total DCs increases with NP treatment groups, with the greatest increase in the (ζ+)NP-treated group. Differences between the composition of the DCs in the lung at this time point are more pronounced. Mice administered (ζ+)NP and (ζ+)NP-OVA yielded an increased percentage of CD11b DCs in the lung, with a corresponding decrease in CD103 percentage. Anionic treatment groups showed considerably less difference, retaining a greater percentage of CD103 DCs than the cationic groups. Overall, there was no difference between PBS and soluble OVA treated groups, indicating the observed responses were NP-driven.

Nanoparticle Trafficking to Mediastinal Lymph Nodes

We further hypothesized that the observed changes in lung populations, local changes in cytokines and chemokines, and differences in APC-NP association would translate to differences in the cellularity and NP frequency in the lung draining LN. 72 hrs after instillation, mediastinal LNs were resected and processed to a single cell suspension and flow cytometry was used to quantify cell and NP frequencies as in the lung. Representative LN gating is shown in Supplemental Figure 5; from this scheme, $CD3^+$ T cells, $CD19^+$ B cells, $CD11c^+$ DCs, and CD11b and CD103 DCs were identified. NP association was determined as before in each cell population by gating by the PBS-treated, NP FMO control, with percentage of NP^+ populations, NP^+ MFI and total NP^+ fluorescence shown in Figure 7.

NP association with APCs in LN cells was unaffected by lung treatment type at this 72 hr time point. Both B and T cells were negative for NP^+ following all treatment types (data not shown). However, between 10-20% of CD103 DCs (Figure 7A) and 5-10% of CD11b DCs (Figure 7B) in the LN were found to be particle positive. However, there were no statistical differences found between the NP^+ percentage within each DC subtype, nor total fluorescence, indicating that NP charge did not influence NP draining to the mediastinal lymph node at this time point. Unlike the lung, there were also no observed differences in the total cellularity of the lymph nodes, or within DC subtypes (Supplemental Figure 6). Macrophage populations were not explored in the draining lymph node, as they are generally considered a lung-resident population (12).

DISCUSSION

As pulmonary delivery of nanoparticles continues to be studied as an approach for the next generation of vaccines, it will be increasingly important to understand how NP properties influence and modify pulmonary immune responses (3, 8). Use of the PRINT platform allowed for the same initial particle hydrogel polymerization, NP geometry, crosslinking network, amount of functional groups, and composition to isolate NP surface charge as the sole variable in these studies. From this, we systematically studied the influence of NP surface charge and antigen attachment on lung APC populations, detailing the cellular distribution of the NPs, cytokine/chemokine production in the lung, changes in lung APC populations, and the propensity to traffic from the lung to the mediastinal LNs. Our results show that cationic NPs are preferentially associated with two important lung DC populations and increase production of important lung chemo-attractants, which may account for their increased efficacy as a pulmonary vaccine carrier.

Cationic NPs preferentially associated with lung DCs, while anionic NPs were more readily internalized by AMs. While AMs are considered APCs, their main function in the lung is to clear and sequester foreign material and maintain lung homeostasis (12, 16, 17). As a result, AMs are not the primary target of NP vaccines and it is more important to target DCs, the “professional” APCs. Importantly, anionic NPs sequestered in AMs would be less successful at eliciting an adaptive immune response, as uptake in AMs represents an efficient lung clearance mechanism. The two lung DC populations studied here have both been implicated in critical immune capabilities, including stimulation of IgA production, $CD4^+$ and $CD8^+$ T

cell priming, and migration to LNs (11, 12, 16, 20-24). As both CD103 and CD11b DCs showed a trend of increased association with cationic NP, it is hypothesized that this increased DC association resulted in the previously reported result from our group demonstrating improved immune response following vaccination with cationic NPs (8). Furthermore, the increased association observed in CD11b DCs may imply an opportunity to skew the overall lung immune status, as CD11b DCs have been implicated as a main mediator of Th2 lung responses (23, 37). These results demonstrate the importance of NP association with lung DCs through manipulation of NP surface chemistry; further cell-targeted delivery may be possible through variation in alternative NP parameters, such as size and surface chemistry (29).

Both NP formulations showed no acute inflammatory response systemically or locally in the BALF. However, further characterization of the lungs for mRNA expression of cytokine or chemokines showed (ζ+)NP administration upregulated genes for two chemokines, CCL2 and CXCL10, responsible for leukocyte recruitment (36, 38). We also detected an increase in total $CD11c^+$ DCs in the lung following cationic NP administration, likely corresponding to the upregulation of these chemokines. Furthermore, the percentage of CD11b DCs from total $CD11c^+$ cells increased, likely due to recruitment of this cell type to the lung, and these cells were most commonly associated to (ζ+)NPs in the lung. Taken together, these data suggest that (ζ+)NP administration to the lung causes recruitment of CD11b DCs to the airways, which then preferentially internalize NPs. This increased recruitment and association alone may account for increased antibody responses previously observed in our group for cationic NPs following pulmonary vaccination, as CD11b cells are the main driver of IgA production (24). Increased responses to (ζ+)NP may also have been enhanced by upregulation of key Th1 cytokines, such as IFN-γ, Il-6, or Il-12, which can contribute to APC activation by 24 hrs (34). It is unclear at this time if this difference in cytokine and chemokine production is a result of interactions with the cationic charge on the NP itself or differences in the total NPs associated, as (ζ+)NPs were more readily associated with DCs than (ζ-)NPs. Aligned with previous studies from our group, (ζ-)NPs were again observed to be immunologically inert in the lung (32). Formulations with such anionic NP carriers lacking an adjuvant stimulus may result in antigen-specific tolerance, which may offer unique therapeutic opportunities (39, 40).

Despite considerable variability in the lung populations and NP cellular association, we do not find that changes in the lung environment have affected trafficking to the LN for the time point or NP parameters tested. Previous work in the literature has shown the role of NP surface charge on passive diffusion from the lung to the LNs, finding that NPs larger than 34 nm do not rapidly translocate from the lung, regardless of surface charge (41). From both whole organ biodistribution, as well as flow cytometry on single cell suspensions of mediastinal LNs, NP fluorescence was detected at similar levels for both anionic and cationic formulations, confirming some degree of NP trafficking from the lung. Thus, we hypothesize that the NPs detected in the LN were actively transported there by lung APCs, which can be further confirmed by using carboxyfluorescein succinimidyl ester (CFSE) or similar staining to selectively label airway cells prior to migration (11, 42). However, no differences were observed in NP association either the LN CD103 DCs, considered to be the main migratory lung population (43), or LN CD11b DC populations. These results are in

contrast from other routes of particle administration, which demonstrated limited trafficking to the local LN of cationic NPs following a foot-pad injection (44). Observation of NP trafficking at longer time points, following multiple NP administrations, or further iterations of NP parameters may yield larger differences in LN trafficking between NP formulations.

While cationic NPs may not be ideal for an intravenous route of administration, their delivery to the lung gives rise to numerous properties which would promote efficacious and safe pulmonary vaccine strategies, and may have implications for other mucosal surfaces as well. Pulmonary vaccination continues to gain attention as a viable approach to protect against wide variety of diseases, especially with increasing developments in dry powder administrations (45, 46). This route offers ease of administration and the elimination of issues associated with traditionally administered vaccines by eliminating cold chain storage issues and requirements for trained personnel for delivery. Additionally, vaccines administered *via* the respiratory tract have demonstrated equivalent or increased local protection in the lung to various pathogens, and can also offer systemic and distal mucosal protection as well (45, 47). The NPs studied here represent a model particle carrier, which can be optimized for a given antigen and route of administration. Our results find that cationic formulations offer superior responses specifically in the lung; these NPs can promote an environment sufficient to promote antigen-specific responses suitable for vaccination, without overt safety concerns. Use of engineered NPs, such as those created through the PRINT platform, allows not only for the optimization of the particle carrier to pulmonary delivery, as shown here, but can be further adapted to carry a range of antigens and antigens to further promote mimicry of the complex pathogen surface (1, 48). This approach is expected to increase the range of pathogens capable of being addressed by pulmonary vaccination.

Overall, these studies are critical in establishing the role of NP properties on pulmonary immune cells, as well as lung APC functions upon particulate exposure. Our findings suggest that cationic NPs may offer increased preference towards lung DC subtypes. Cationic formulations not only resulted in increased DC association, but modulated the local lung environment to promote recruitment and maturation of lung DCs, while avoiding extensive AM clearance. In contrast, anionic formulations were found to be immunologically inert in the lung, which may offer alternative therapeutic options towards promoting tolerance. Our findings demonstrate the importance of particle surface charge in pulmonary NP vaccine design and will hopefully contribute to the design of novel vaccines towards a wide range of pulmonary pathogens.

Supplementary Material

Refer to Web version on PubMed Central for supplementary material.

ACKNOLWEDGEMENTS

We thank K. Reuter, A. Pandya, B. Cadenas, and A. Azcarate-Peril for useful discussions and technical assistance. We acknowledge Liquidia Technologies for providing PRINT molds, and the core facilities at UNC, including the LCCC Histopathology Core, the Department of Microbiology and Immunology Flow Cytometry Core, the Microbiome Core Facility, and DLAM facility.

Funding: This work was funded in part by the NIH Pioneer Award to J.M.D. (1DP1OD006432), DTRA award (HDTRA1-13-1-0045) and the NSF Graduate Research Fellowship, as well as NCI Center Core Support Grant CA016086.

LIST OF ABBREVIATIONS

BALF	Bronchoalveolar lavage fluid
DC	Dendritic cell
AM	Alveolar macrophage
NP	Nanoparticle
APC	Antigen presenting cell
MHC	Major histocompatibility complex
LN	Lymph node
PRINT	Particle replication in non-wetting templates
IACUC	Institutional Animal Care and Use Committee
OVA	Ovalbumin
LPS	Lipopolysaccharide
RT-qPCR	Quantitative reverse transcription polymerase chain reaction
FMO	Fluorescence minus one
MFI	Median fluorescence intensity
ELISA	Enzyme-linked immunosorbent assay
H&E	Hematoxylin and eosin
FI	Fluorescence intensity
TLR	Toll-like receptor
CFSE	Carboxyfluorescein succinimidyl ester
(ζ+)NP	Cationic nanoparticle
Tgf-β1	Transforming growth factor beta one
Tnf-α	Tumor necrosis factor alpha
Il	Interleukin
Inf-γ	Interferon gamma
Cxcl	Chemokine (C-X-C motif) ligand
Ccl	Chemokine (C-C motif) ligand
Gapdh	Glyceraldehyde-3-Phosphate Dehydrogenase

REFERENCES

1. Garcia A, Mack P, Williams S, Fromen C, Shen T, Tully J, Pillai J, Kuehl P, Napier M, Desimone JM, Maynor BW. Microfabricated engineered particle systems for respiratory drug delivery and

other pharmaceutical applications. Journal of drug delivery. 2012; 2012:941243. [PubMed: 22518316]

2. Blank F, Stumbles P, von Garnier C. Opportunities and challenges of the pulmonary route for vaccination. Expert Opin Drug Deliv. 2011; 8:547–563. [PubMed: 21438741]
3. Moon JJ, Huang B, Irvine DJ. Engineering nano- and microparticles to tune immunity. Adv Mater. 2012; 24:3724–3746. [PubMed: 22641380]
4. Li AV, Moon JJ, Abraham W, Suh H, Elkhader J, Seidman MA, Yen M, Im E, Foley MH, Barouch DH, Irvine DJ. Generation of effector memory t cell-based mucosal and systemic immunity with pulmonary nanoparticle vaccination. Sci Transl Med. 2013; 5:204–130.
5. Nembrini C, Stano A, Dane KY, Ballester M, van der Vlies AJ, Marsland BJ, Swartz MA, Hubbell JA. Nanoparticle conjugation of antigen enhances cytotoxic t-cell responses in pulmonary vaccination. Proceedings of the National Academy of Sciences of the United States of America. 2011; 108:E989–997. [PubMed: 21969597]
6. Smith DM, Simon JK, Baker JR Jr. Applications of nanotechnology for immunology. Nature reviews Immunology. 2013; 13:592–605.
7. Pulliam B, Sung JC, Edwards DA. Design of nanoparticle-based dry powder pulmonary vaccines. Expert Opin Drug Deliv. 2007; 4:651–663. [PubMed: 17970667]
8. Fromen CA, Robbins GR, Shen TW, Kai MP, Ting JPY, DeSimone JM. Controlled analysis of nanoparticle charge on mucosal and systemic antibody responses following pulmonary immunization. Proceedings of the National Academy of Sciences. 2014:201422923.
9. Fromen CA, Shen TW, Larus AE, Mack P, Maynor BW, Luft JC, DeSimone JM. Synthesis and characterization of monodisperse uniformly shaped respirable aerosols. AIChE Journal. 2013; 59:3184–3194.
10. Kunda NK, Somavarapu S, Gordon SB, Hutcheon GA, Saleem IY. Nanocarriers targeting dendritic cells for pulmonary vaccine delivery. Pharmaceutical research. 2013; 30:325–341. [PubMed: 23054093]
11. Sakagami M. In vivo, in vitro and ex vivo models to assess pulmonary absorption and disposition of inhaled therapeutics for systemic delivery. Advanced drug delivery reviews. 2006; 58:1030–1060. [PubMed: 17010473]
12. Guilliams M, Lambrecht BN, Hammad H. Division of labor between lung dendritic cells and macrophages in the defense against pulmonary infections. Mucosal immunology. 2013; 6:464–473. [PubMed: 23549447]
13. Azarmi S, Roa WH, Lobenberg R. Targeted delivery of nanoparticles for the treatment of lung diseases. Advanced drug delivery reviews. 2008; 60:863–875. [PubMed: 18308418]
14. Hassan MS, Lau RW. Effect of particle shape on dry particle inhalation: Study of flowability, aerosolization, and deposition properties. AAPS PharmSciTech. 2009; 10:1252–1262. [PubMed: 19866362]
15. Kleinstreuer C, Zhang Z, Li Z, Roberts WL, Rojas C. A new methodology for targeting drug-aerosols in the human respiratory system. International Journal of Heat and Mass Transfer. 2008; 51:5578–5589.
16. Hardy CL, Lemasurier JS, Mohamud R, Yao J, Xiang SD, Rolland JM, O'Hehir RE, Plebanski M. Differential uptake of nanoparticles and microparticles by pulmonary apc subsets induces discrete immunological imprints. J Immunol. 2013; 191:5278–5290. [PubMed: 24123688]
17. Fernandes CA, Vanbever R. Preclinical models for pulmonary drug delivery. Expert Opin Drug Deliv. 2009; 6:1231–1245. [PubMed: 19852680]
18. Thiel CG. Can in vitro particle size measurements be used to predict pulmonary deposition of aerosol from inhalers? J Aerosol Med. 1998; 11:S43–S52. [PubMed: 10180732]
19. Inaba K, Steinman RM, Van Voorhis WC, Muramatsu S. Dendritic cells are critical accessory cells for thymus-dependent antibody responses in mouse and in man. Proceedings of the National Academy of Sciences of the United States of America. 1983; 80:6041–6045. [PubMed: 6351074]
20. Naito T, Suda T, Suzuki K, Nakamura Y, Inui N, Sato J, Chida K, Nakamura H. Lung dendritic cells have a potent capability to induce production of immunoglobulin a. American journal of respiratory cell and molecular biology. 2008; 38:161–167. [PubMed: 17709597]

21. Xie Y, Zeng P, Wiedmann TS. Disease guided optimization of the respiratory delivery of microparticulate formulations. Expert Opin Drug Deliv. 2008; 5:269–289. [PubMed: 18318650]
22. Abdelwahed W, Degobert G, Stainmesse S, Fessi H. Freeze-drying of nanoparticles: Formulation, process and storage considerations. Advanced drug delivery reviews. 2006; 58:1688–1713. [PubMed: 17118485]
23. Furuhashi K, Suda T, Hasegawa H, Suzuki Y, Hashimoto D, Enomoto N, Fujisawa T, Nakamura Y, Inui N, Shibata K, Nakamura H, Chida K. Mouse lung cd103+ and cd11bhigh dendritic cells preferentially induce distinct cd4+ t-cell responses. American journal of respiratory cell and molecular biology. 2012; 46:165–172. [PubMed: 21908266]
24. Suzuki Y, Suda T, Furuhashi K, Shibata K, Hashimoto D, Enomto N, Fujisawa T, Nakamura Y, Inui N, Nakamura H, Chida K. Mouse cd11bhigh lung dendritic cells have more potent capability to induce iga than cd103+ lung dendritic cells in vitro. American journal of respiratory cell and molecular biology. 2012; 46:773–780. [PubMed: 22268142]
25. Zhao L, Seth A, Wibowo N, Zhao CX, Mitter N, Yu C, Middelberg AP. Nanoparticle vaccines. Vaccine. 2014; 32:327–337. [PubMed: 24295808]
26. Michen B, Graule T. Isoelectric points of viruses. Journal of applied microbiology. 2010; 109:388–397. [PubMed: 20102425]
27. van der Mei HC, Busscher HJ. Bacterial cell surface heterogeneity: A pathogen's disguise. PLOS Pathogens. 2012; 8:e1002821. [PubMed: 22952444]
28. Perry JL, Reuter KG, Kai MP, Herlihy KP, Jones SW, Luft JC, Napier M, Bear JE, DeSimone JM. Pegylated print nanoparticles: The impact of peg density on protein binding, macrophage association, biodistribution, and pharmacokinetics. Nano letters. 2012; 12:5304–5310. [PubMed: 22920324]
29. Shen TW, Fromen CA, Kai MP, Luft JC, Rahhal TB, Robbins GR, DeSimone JM. Distribution and cellular uptake of pegylated polymeric particles in the lung towards cell-specific targeted delivery. Pharmaceutical research. 2015
30. Robbins GR, Truax AD, Davis BK, Zhang L, Brickey WJ, Ting JP. Regulation of class i major histocompatibility complex (mhc) by nucleotide-binding domain, leucine-rich repeat-containing (nlr) proteins. The Journal of biological chemistry. 2012; 287:24294–24303. [PubMed: 22645137]
31. Mitchell JP, Nagel MW. Cascade impactors for the size characterization of aerosols from medical inhalers. J Aerosol Med. 2003; 16:341–377. [PubMed: 14977427]
32. Roberts RA, Shen T, Allen IC, Hasan W, DeSimone JM, Ting JP. Analysis of the murine immune response to pulmonary delivery of precisely fabricated nano- and microscale particles. PloS one. 2013; 8:e62115. [PubMed: 23593509]
33. Johnston CJ, Finkelstein JN, Gelein R, Oberdorster G. Pulmonary cytokine and chemokine mrna levels after inhalation of lipopolysaccharide in c57bl/6 mice. Toxicological Sciences. 1998; 46:300–307. [PubMed: 10048133]
34. Pesce I, Monaci E, Muzzi A, Tritto E, Tavarini S, Nuti S, De Gregorio E, Wack A. Intranasal administration of cpg induces a rapid and transient cytokine response followed by dendritic and natural killer cell activation and recruitment in the mouse lung. Journal of innate immunity. 2010; 2:144–159. [PubMed: 20375632]
35. Rose CE Jr. Sung SS, Fu SM. Significant involvement of ccl2 (mcp-1) in inflammatory disorders of the lung. Microcirculation. 2003; 10:273–288. [PubMed: 12851645]
36. Deshmane SL, Kremlev S, Amini S, Sawaya BE. Monocyte chemoattractant protein-1 (mcp-1): An overview. Journal of interferon & cytokine research : the official journal of the International Society for Interferon and Cytokine Research. 2009; 29:313–326.
37. Larhrib H, Martin GP, Marriott C, Prime D. The influence of carrier and drug morphology on drug delivery from dry powder formulations. International Journal of Pharmaceutics. 2003; 257:283–296. [PubMed: 12711183]
38. Dong S, Zhang X, He Y, Xu F, Li D, Xu W, Wang H, Yin Y, Cao J. Synergy of il-27 and tnf-alpha in regulating cxcl10 expression in lung fibroblasts. American journal of respiratory cell and molecular biology. 2013; 48:518–530. [PubMed: 23333920]
39. Cook DN, Bottomly K. Innate immune control of pulmonary dendritic cell trafficking. Proceedings of the American Thoracic Society. 2007; 4:234–239. [PubMed: 17607005]

40. Smarr CB, Hsu CL, Byrne AJ, Miller SD, Bryce PJ. Antigen-fixed leukocytes tolerize th2 responses in mouse models of allergy. J Immunol. 2011; 187:5090–5098. [PubMed: 21976774]

41. Choi HS, Ashitate Y, Lee JH, Kim SH, Matsui A, Insin N, Bawendi MG, Semmler-Behnke M, Frangioni JV, Tsuda A. Rapid translocation of nanoparticles from the lung airspaces to the body. Nature biotechnology. 2010; 28:1300–1303.

42. Pal I, Ramsey JD. The role of the lymphatic system in vaccine trafficking and immune response. Advanced drug delivery reviews. 2011; 63:909–922. [PubMed: 21683103]

43. Blank F, Stumbles PA, Seydoux E, Holt PG, Fink A, Rothen-Rutishauser B, Strickland DH, von Garnier C. Size-dependent uptake of particles by pulmonary antigen-presenting cell populations and trafficking to regional lymph nodes. American journal of respiratory cell and molecular biology. 2013; 49:67–77. [PubMed: 23492193]

44. Mueller SN, Tian S, DeSimone JM. Rapid and persistent delivery of antigen by lymph node targeting print nanoparticle vaccine carrier to promote humoral immunity. Molecular pharmaceutics. 2015; 12:1356–1365. [PubMed: 25817072]

45. Tonnis WF, Kersten GF, Frijlink HW, Hinrichs WLJ, de Boer AH, Amorij J. Pulmonary vaccine delivery: A realistic approach? Journal of aerosol medicine and pulmonary drug delivery. 2012; 25:249–260. [PubMed: 22856876]

46. Sou T, Meeusen EN, de Veer M, Morton DA, Kaminskas LM, McIntosh MP. New developments in dry powder pulmonary vaccine delivery. Trends in biotechnology. 2011; 29:191–198. [PubMed: 21255854]

47. Neutra MR, Kozlowski PA. Mucosal vaccines: The promise and the challenge. Nature reviews Immunology. 2006; 6:148–158.

48. Galloway AL, Murphy A, DeSimone JM, Di J, Herrmann JP, Hunter ME, Kindig JP, Malinoski FJ, Rumley MA, Stoltz DM, Templeman TS, Hubby B. Development of a nanoparticle-based influenza vaccine using the print technology. Nanomedicine : nanotechnology, biology, and medicine. 2013; 9:523–531.

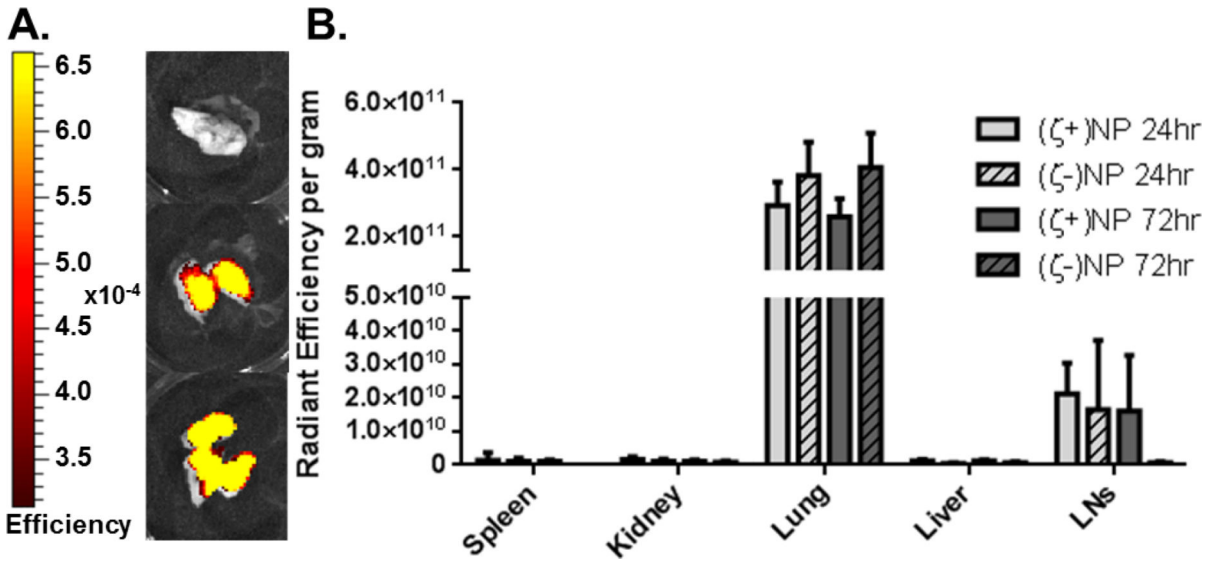

Figure 1.

Biodistribution of Instilled Nanoparticles. (A) Representative IVIS imaging. From top to bottom: Saline, (ζ+)NP, and (ζ-)NP negative at 24 hrs. Scale bar ranges from 3.14e-4 to 6.61e-4. (B) Organ distribution of instilled nanoparticles at 24 and 72 hrs. n=4 with bar representing SD. Statistics performed by 1-way ANOVA within groups with Tukey multiple comparisons test, n.s.

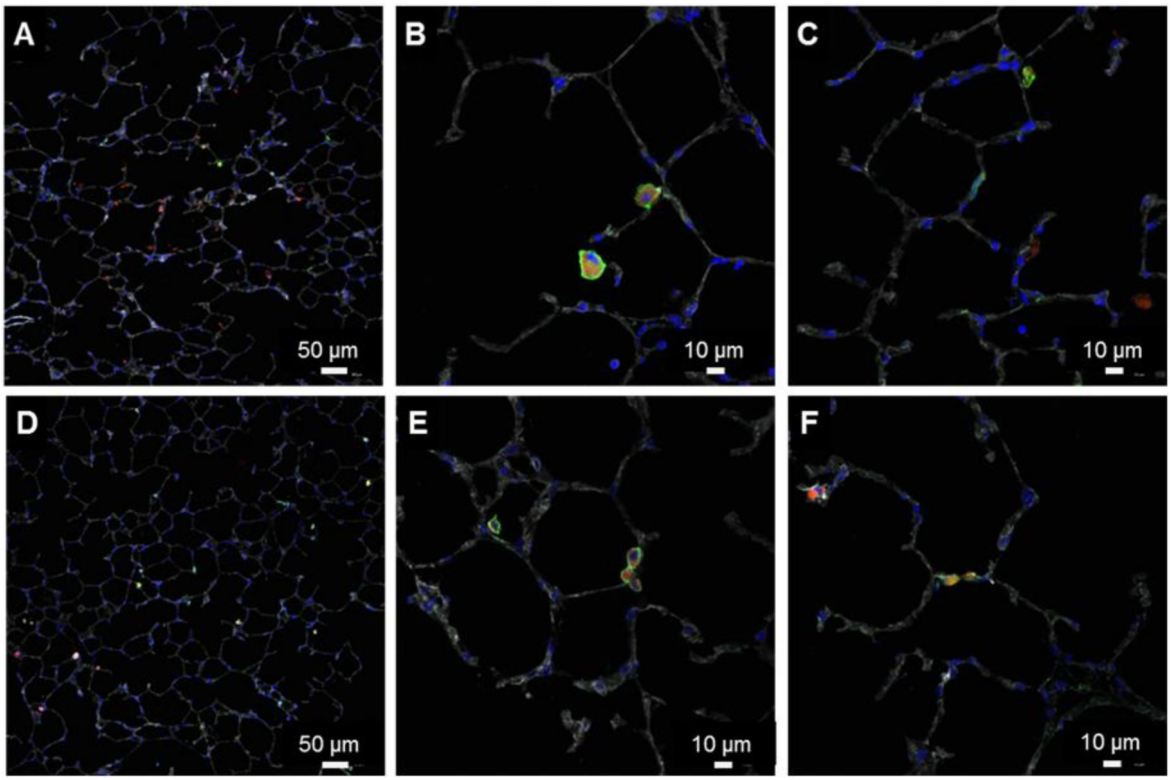

Figure 2.

Representative immunohistochemistry of NP-treated lungs after 72 hrs. Sections stained for fluorescent NPs (red), phalloidin (gray), DAPI (blue), and $CD11c^+$ (green). (A-C) (ζ+) NPs. (D-F) (ζ-) NPs.

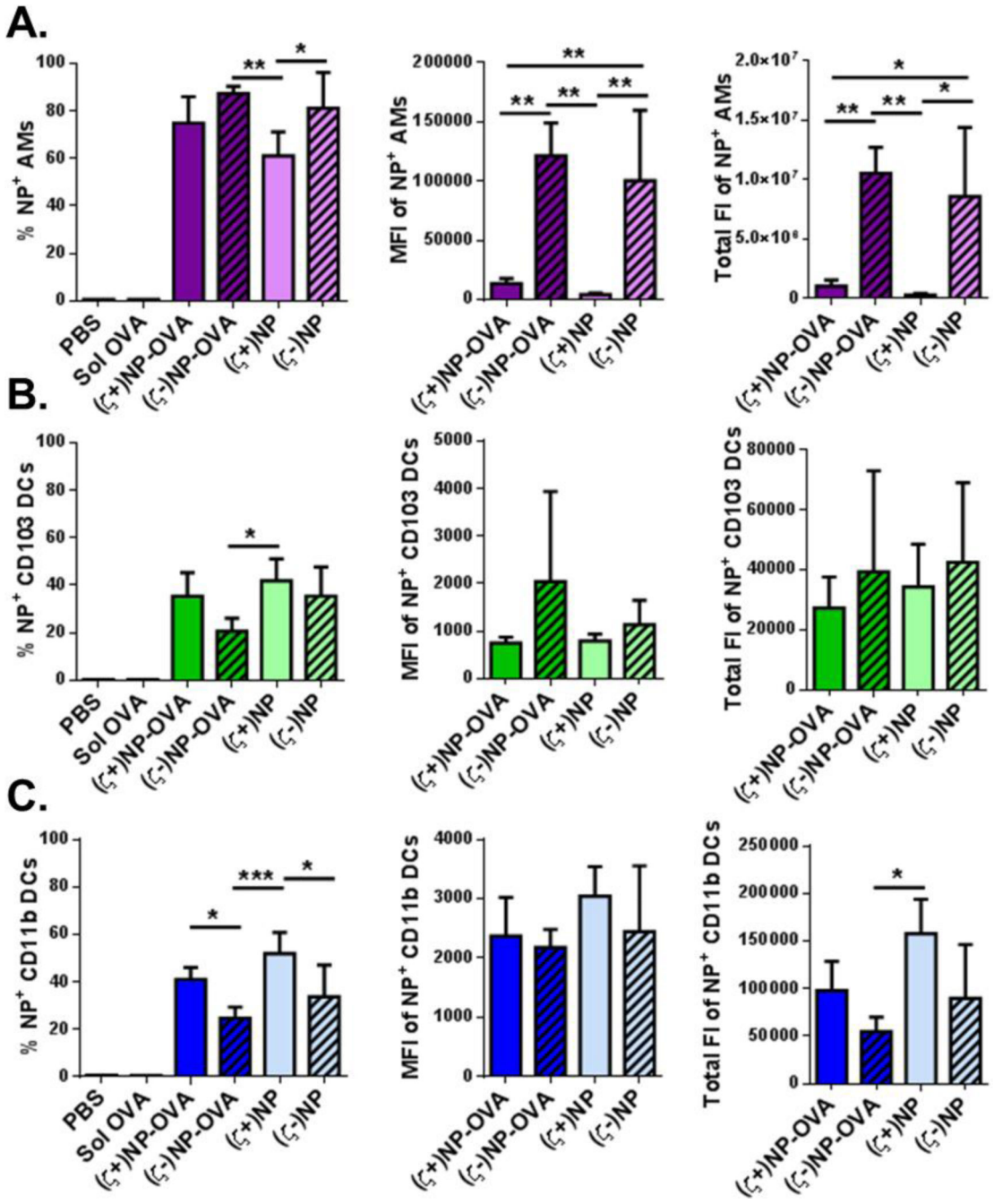

Figure 3.

NP association in lung APCs. NPs association in (A) AMs, (B) CD103 DCs and (C) CD11b DCs from whole lungs of treated C57BL/6 mice after 72 hrs, n≥4 with bar representing SD. Within each population, graphs from left to right show the percent NP positive cells, MFI of positive cells, and total fluorescence of that cell type. Statistics performed by 1-way ANOVA with Tukey multiple comparisons test with *p≤0.05, **p≤0.01, ***p≤0.001. Representative gating is found in Supplemental Figure 1.

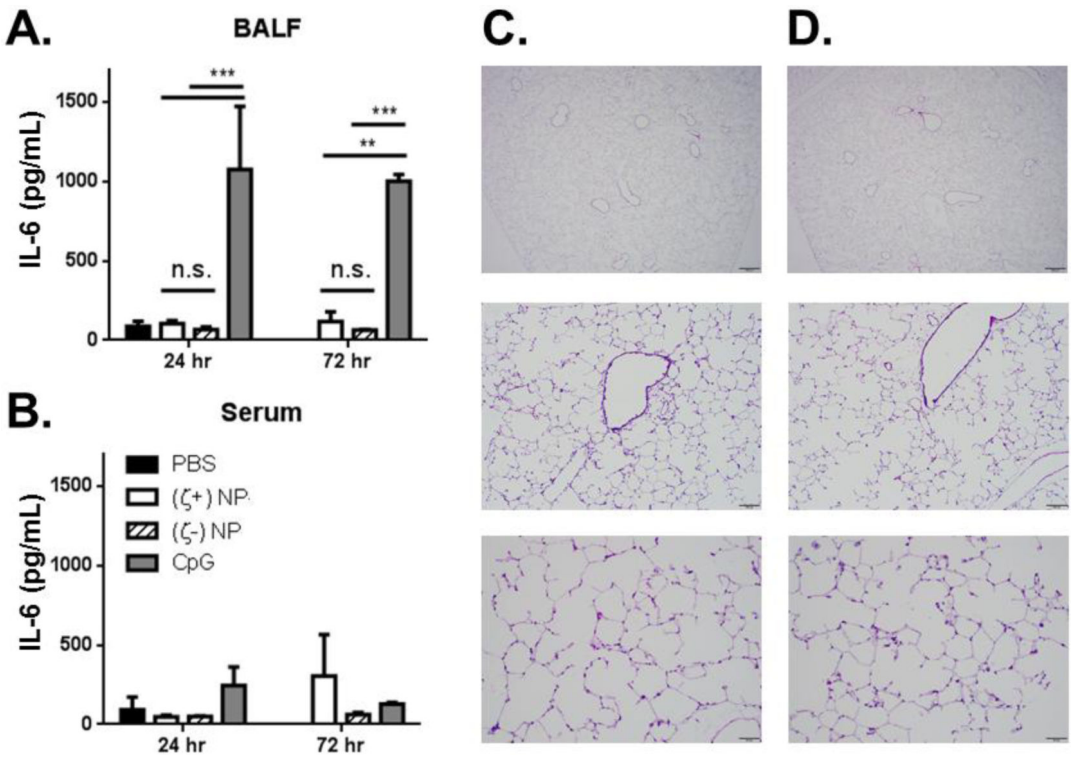

Figure 4.

IL-6 cytokine analysis of (A) BALF and (B) serum following NP and CpG instillation at 24 and 72 hrs in C57BL/6 mice, n=3 with bar representing SD. Statistics performed by 2-way ANOVA with Tukey multiple comparisons test with **p≤0.01, ***p≤0.001. (C & D) H&E stained whole lung sections of NP treated lungs at three magnifications: (C) shows (ζ+)NP treated and (D) shows (ζ-)NP treated at 24 hrs following NP instillation with scale bars (from top to bottom) of 500 μm, 100 μm, and 50 μm, respectively.

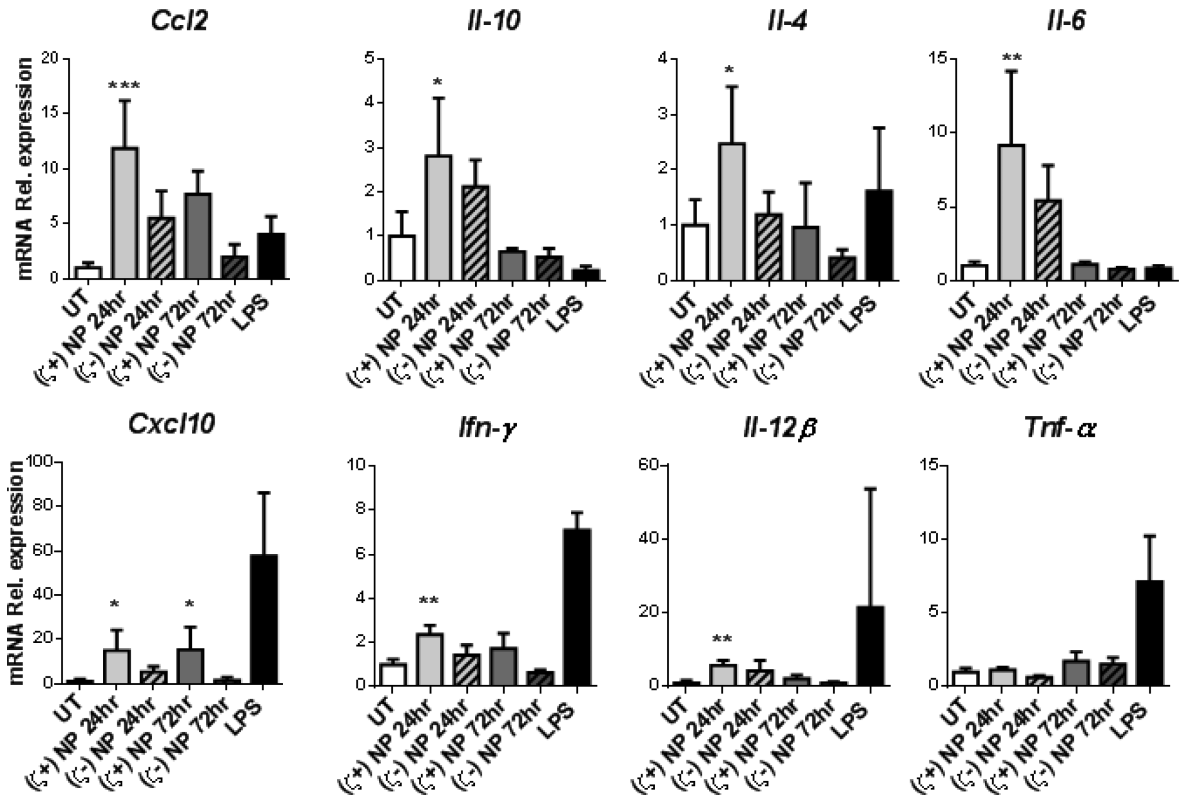

Figure 5.

qRT-PCR for mRNA expression of *Ccl2, Il-10, Il-4, Il-6, Cxcl10, Ifn-γ, Il-12β,* and *Tnf-α* by single cell suspensions of lung cells treated with either (ζ+)NP or (ζ-)NP and homogenized at 24 hrs and 72 hrs. Data are normalized to *GADPH* mRNA (quantity shown in Supplemental Figure 3) and graphed as fold change over UT. UT and LPS treatments shown for 24 hrs. n=4 with bar representing SD. Statistics performed by 1-way ANOVA with Dunnet's multiple comparisons test to UT control with *p≤0.05, **p≤0.01, ***p≤0.001 and LPS groups excluded from statistical analysis.

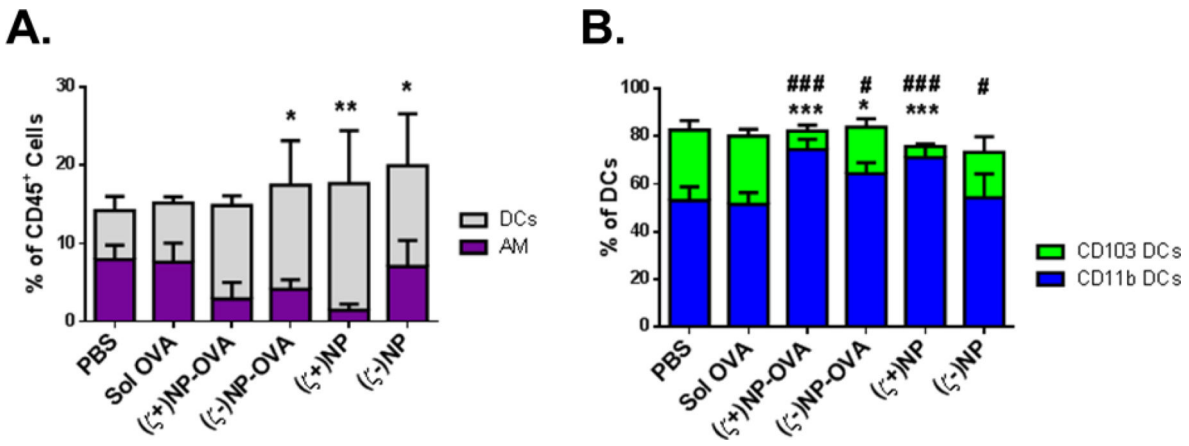

Figure 6.

APC populations in the lung following NP treatment. (A) APC population breakdown of DCs and APCs in the whole lungs of treated C57BL/6 mice after 72 hrs, n≥4 with bar representing SD. Populations stacked and not overlaid, such that bar magnitude as shown represents the sum of two cell populations. Statistics performed by 1-way ANOVA with Dunnet's multiple comparisons test to PBS treatment. *indicate significant difference within DCs with *p≤0.05, **p≤0.01, ***p≤0.001, AM n.s between groups. Populations stacked. (B) Subtypes of $CD11c^+$ DCs in the whole lungs of treated C57BL/6 mice after 24 hrs, n≥4 with bar representing SD. Statistics performed by 1-way ANOVA with Dunnet's multiple comparisons test to PBS treatment. * indicate significant difference within CD11b DCs compared to PBS with *p≤0.05, **p≤0.01, ***p≤0.001 and # indicate significant difference within CD103 DCs compared to PBS with #p≤0.05, ##p≤0.01, ###p≤0.001. Representative gating is found in Supplemental Figure 1.

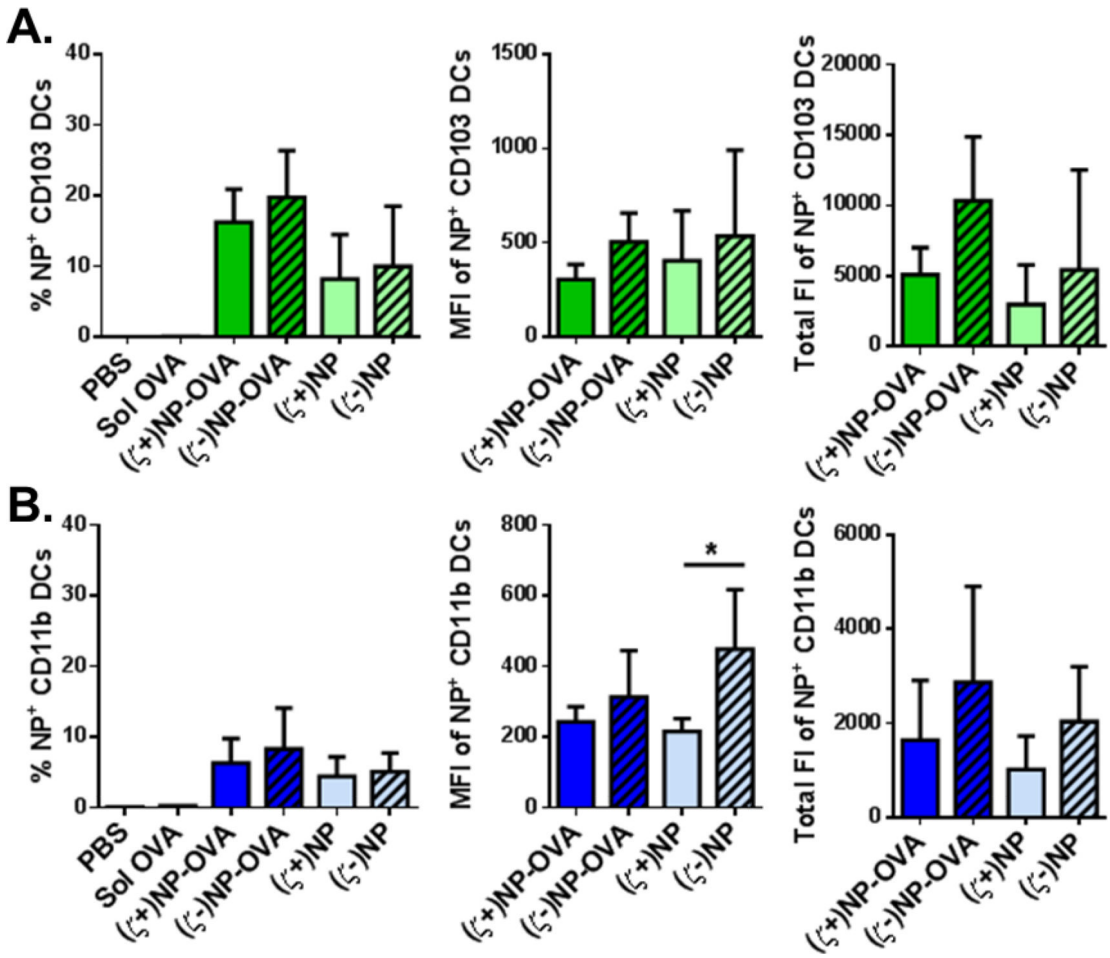

Figure 7.

NP association in LN DCs. NPs association in (A) CD103 DCs, and (B) CD11b DCs from mediastinal LNs of treated C57BL/6 mice after 72 hrs, n≥4 with bar representing SD. Within each population, graphs from left to right show the percent NP positive cells, MFI of positive cells, and total fluorescence of that cell type. Statistics performed by 1-way ANOVA with Tukey multiple comparisons test with *p≤0.05. Representative gating is found in Supplemental Figure 5.